



## Covalent organic framework as an efficient, metal-free, heterogeneous photocatalyst for organic transformations under visible light



Ziping Li<sup>a</sup>, Yongfeng Zhi<sup>a</sup>, Pengpeng Shao<sup>c</sup>, Hong Xia<sup>b</sup>, Guosheng Li<sup>e</sup>, Xiao Feng<sup>c</sup>, Xiong Chen<sup>e</sup>, Zhan Shi<sup>d</sup>, Xiaoming Liu<sup>a,\*</sup>

<sup>a</sup> College of Chemistry, Jilin University, Changchun, 130012, PR China

<sup>b</sup> State Key Laboratory on Integrated Optoelectronics, College of Electronic Science and Technology, Jilin University, Changchun, 130012, PR China

<sup>c</sup> School of Chemistry, Beijing Institute of Technology, Beijing, 100081, PR China

<sup>d</sup> State Key Laboratory of Inorganic Synthesis and Preparative Chemistry, College of Chemistry, Jilin University, Changchun, 130012, PR China

<sup>e</sup> State Key Laboratory of Photocatalysis on Energy and Environment, College of Chemistry, Fuzhou University, Fuzhou, 350002, PR China

### ARTICLE INFO

#### Keywords:

Covalent organic frameworks  
Heterogeneous catalysis  
Photocatalysis  
Metal-free  
Visible light

### ABSTRACT

Visible-light active, heterogeneous, and organic photocatalysts exhibit a more sustainable and environmentally friendly alternative to classical metal-based catalysts. Two-dimensional covalent organic frameworks (2D-COFs) with permanent porosity, columnar  $\pi$ -arrays and excellent stability, that can become an excellent platform for heterogeneous photocatalysis of organic transformations. Here we report a predesigned imine-based COF with electron donor and acceptor structure. And new framework possesses large surface area, high crystallinity, outstanding stability and broad absorption range in the visible-light region as well as good photoelectric response characteristics. Importantly, it was found to be a highly effective heterogeneous photocatalyst for reductive dehalogenation of phenacyl bromide derivatives and  $\alpha$ -alkylation of aldehydes under irradiation of visible-light. In addition, the COF gave good recyclability and could be reused after a simple separation manipulation. The current present still reveals a great prospect for 2D-COFs as metal-free, heterogeneous photocatalysts for organic transformations.

### 1. Introduction

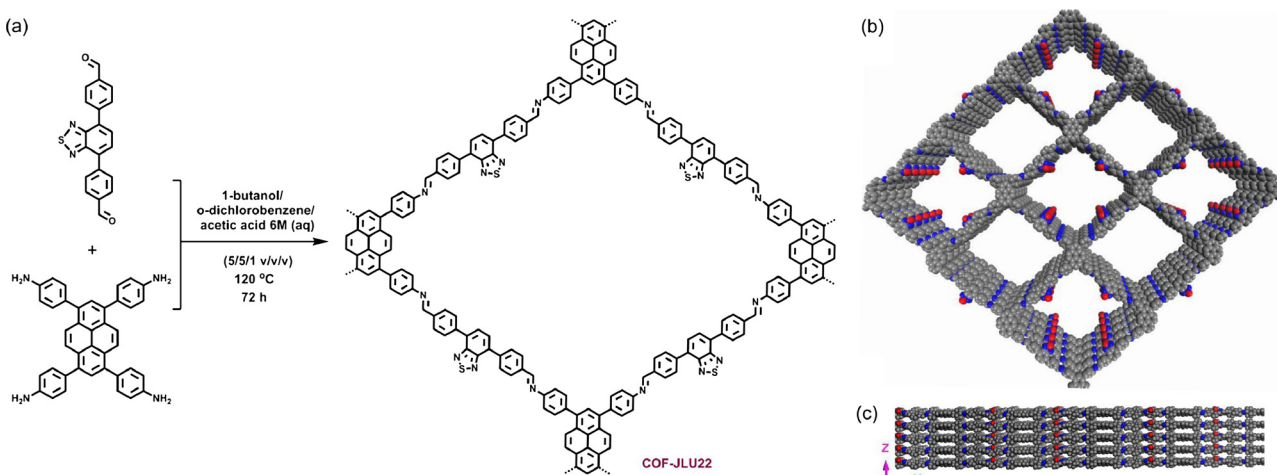
During the past decade, the use of visible light to drive organic transformations has attracted huge attention due to concerns over the simple, mild and environmentally friendly process as well as a sustainable way for efficient preparation of fine chemicals [1–3]. The design and construction of photocatalysts has always maintained a core position in photocatalysis research, which focuses on improving the photocatalytic performance. Up to now, various photocatalytic systems including inorganic semiconductors [4], organometal complexes [5,6] and pure organic dyes [7] have been widely investigated in photoredox reactions owing to their intense absorption and rich redox features in the excited state. Recently, some polymer-based photocatalysts such as graphitic carbon nitride [8,9] metal-organic frameworks [10], and dye sensitized mesoporous silica [11] have been researched for many kinds of photocatalytic organic transformations, in order to overcome the important deficiencies of the aforementioned homogeneous photocatalysts involving high cost, tedious separation and low reusability. In particular, covalently linked porous organic polymers (POPs) have

emerged as metal-free, recyclable heterogeneous photocatalysts with a highly catalytic efficiency under visible-light irradiation and shown great potential in organic synthesis [12–17].

As a novel class of crystalline porous organic polymer materials, covalent organic frameworks (COFs) are constructed from organic building blocks under reticular chemistry, and exhibit intriguing aesthetic architectures and permanent porosity. The most important feature of COFs is that it is easy to realize the regulation of the framework structure and functionality [18]. Benefit from the combination of large specific surface area, extremely low density, good thermal and chemical stability, COFs have emerged as promising platforms for potential applications in gas adsorption [19,20], sensing [21–23], energy storage [24], and heterogeneous catalysis [25–29]. For two-dimensional (2D) networks, they possess periodic columnar  $\pi$ -arrays and 1D nanopores originating from layered stacking of 2D macromolecular sheets. The ordered and conductive columns provide an ideal channel for the separation, diffusion, and migration of the photogenerated electron-hole pairs. From the point of view of structure, therefore, the photoactive 2D-COFs can be powerful candidates in optoelectronic devices [30] and

\* Corresponding author.

E-mail address: [xm\\_liu@jlu.edu.cn](mailto:xm_liu@jlu.edu.cn) (X. Liu).



**Scheme 1.** (a) Synthesis of COF-JLU22 by imine condensation reaction. (b) Top and (c) side views of COF-JLU22 (red, sulfur; blue, nitrogen; gray, carbon; hydrogen is omitted for clarity). (For interpretation of the references to colour in this figure legend, the reader is referred to the web version of this article.)

photocatalysis [31–34]. Indeed, a pioneering research by the Lotsch group has reported a 2D hydrazone-based COF for photocatalytic hydrogen evolution under visible-light [35]. Until now, however, the study of 2D-COFs as heterogeneous photocatalysts for organic synthesis is still rare [36,37].

To obtain an ideal COF-based photocatalyst for organic synthesis, the structure was predesigned in detail. On the one hand, using 1,3,6,8-tetrakis(4-aminophenyl)pyrene as a knot, due to pyrene-based COFs have not only large specific surface area, strong crystallinity and excellent stability [38,39], but also pyrene-based compounds possess good photoelectric activity [40]. On the other hand, a longer linker with highly electron deficiency, 4,7-diphenylbenzo[c][1,2,5]thiadiazole, was introduced into the framework resulting in the formation of mesoporous channels, which is beneficial to improve the reaction and transmission rate of the matter. Furthermore, the construction of the electronic donor-acceptor type COF can effectively red-shift absorption wavelengths and enhance the photocatalytic activity of the COF [16,17,39]. Herein, we report a novel pyrene-based 2D-COF with high surface area and large pore volume, strong crystallinity and robust stability (Scheme 1, COF-JLU22), and its photoelectric properties including adsorption, emission, optical bandgaps, energy levels and transient photocurrent response as well as photocatalytic activity were investigated carefully. Indeed, the COF-JLU22 can serve as a metal-free, recyclable photocatalyst with high catalytic efficiency for reductive dehalogenation of phenacyl bromide derivatives and  $\alpha$ -alkylation of aldehydes under visible-light irradiation. And the mechanism responsible for COF-JLU22 for both organic reactions was still full investigated.

## 2. Experiments

### 2.1. Synthesis of COF-JLU22

An *o*-DCB/*n*-BuOH (0.5 mL/0.5 mL) mixture of 1,3,6,8-tetrakis(4-aminophenyl)pyrene (11.3 mg, 0.02 mmol) and 4,4'-(benzothiadiazole-4,7-diyl) dibenzaldehyde (13.7 mg, 0.04 mmol) in the presence of an acetic acid catalyst (0.1 mL, 6 M) in a 10-mL Pyrex tube was degassed for three times. The tube was flame-sealed and heated at 120 °C for three days. The precipitate was collected through centrifugation, washed with anhydrous acetone (3 × 5 mL) and anhydrous THF (3 × 5 mL). The powder was collected and dried at 120 °C under vacuum overnight to produce COF-JLU22 as a red solid in 90% isolated yield. Anal. Calcd for (C<sub>40</sub>H<sub>23</sub>N<sub>4</sub>S)<sub>n</sub>: C 81.19; H 3.92; N 9.47; S 5.42. Found: C 78.60; H 4.14; N 8.85; S 4.93.

### 2.2. Characterization

The infrared spectra were recorded from 400 to 4000  $\text{cm}^{-1}$  on an Avatar FT-IR 360 spectrometer by using KBr pellets. <sup>1</sup>H spectra were recorded on a Avance III-400 NMR spectrometer, where chemical shifts ( $\delta$  in ppm) were determined with a residual proton of the solvent as standard. Solid-state <sup>1</sup>H MAS NMR and <sup>13</sup>C CP/MAS NMR measurement was recorded using a Bruker AVANCE III 400 WB spectrometer at a MAS rate of 5 kHz and a CP contact time of 2 ms. Elemental analyses were carried out on an Elementar model vario EL cube analyzer. UV/vis spectra have been carried out on a Shimadzu Corporation U-4100 Spectrophotometer within the wavelength range 200–800 nm. Field emission scanning electron microscopy was performed on a SU8020 model HITACHI microscope. Transmission electron microscopy was performed on a JEOL model JEM-2100 microscope. The sample was prepared by drop-casting a supersonicated methanol suspension of COF-JLU22 onto a copper grid. Powder X-ray diffraction data were recorded on a PANalytical BV Empyrean diffractometer by depositing powder on glass substrate, from  $2\theta = 1.5^\circ$  to  $45^\circ$  with  $0.02^\circ$  increment at 25 °C. Thermogravimetric analysis (TGA) was performed on a TA Q500 thermogravimeter by measuring the weight loss while heating at a rate of 10 °C  $\text{min}^{-1}$  from room temperature to 800 °C under nitrogen. Nitrogen sorption isotherms were measured at 77 K with a JW-BK 132F analyzer. Before measurement, the samples were degassed in vacuum at 120 °C for more than 10 h. The Brunauer–Emmett–Teller (BET) method was utilized to calculate the specific surface areas and pore volume. The nonlocal density functional theory (NLDFT) method was applied for the estimation of pore size distribution. The fluorescence emission spectrum were measured on an Edinburgh FLS920 steady state spectrometer by depositing powder on glass substrate. The catalytic products were quantified by GC analysis (Shimadzu GC-2014C) using an SE-54 column (30 m × 0.25 mm × 0.25 mm). The EPR spectra were recorded on a JEOL JES-FA200 EPR spectrometer. Samples were quantitatively injected into specially made quartz capillaries for ESR analysis. The data of diethyl bromomalonate (0.5 M) and PBN solution (0.1 M) were collected under this instrument parameters: scanning frequency, 9438.38 MHz; central field, 337 mT; scanning width, 100 G; scanning power, 5 mW; scanning temperature: 298 K; scanning time, 60 s. All the irradiations were performed with 520 nm continuous laser. The valence band X-ray photoelectron spectroscopy (VB-XPS) measurements were performed on a Thermo ESCALAB 250 Electron spectrometer using Al K $\alpha$  radiation as the X-ray source.

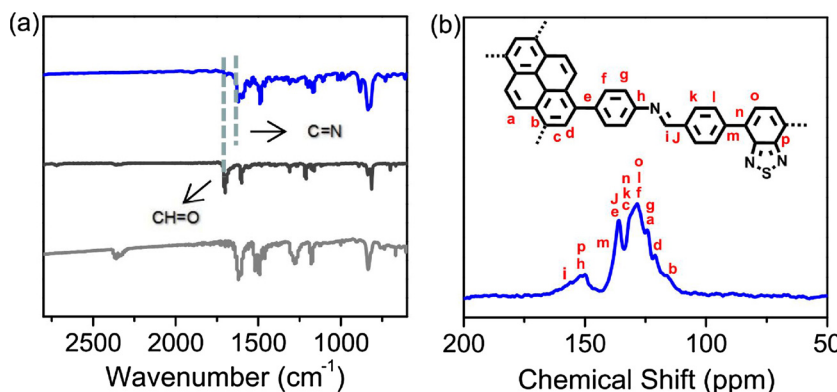


**Fig. 1.** (a) FT-IR spectra of 1,3,6,8-tetrakis(4-aminophenyl)pyrene (gray line), 4,4'-(Benzothiadiazole-4,7-diyl) dibenzaldehyde (black line) and COF-JLU22 (blue line). (b) Solid state <sup>13</sup>C CP/MAS NMR spectrum of COF-JLU22. (For interpretation of the references to colour in this figure legend, the reader is referred to the web version of this article.)

### 2.3. Electrochemical measurements

Electrochemical measurements were performed in a three-electrode system with a VersaSTAT 3 electrochemical workstation (AMETEK Scientific Instruments, USA). The glass carbon electrode (GCE) was used as working electrode, a platinum wire electrode, and a saturated calomel electrode (SCE) as counter and reference electrode, respectively. To create measurable polymer films, the polymer was mixed and ground with 5.0 wt% Nafion, the mixture was dropped on top of a glassy carbon working electrode, and the solvents were evaporated in a vacuum oven for at least 30 min. The measurements were carried out in a 0.1 M solution of tetrabutylammonium hexafluorophosphate in acetonitrile. A Pt counter electrode and a SCE reference electrode were used. Scan rate: 100 mV s<sup>-1</sup>, T = 25 °C. The photocurrent of the polymer was measured on VersaSTAT 3 electrochemical workstation under UV-vis light irradiation with 25 s light on-off cycles. The working electrode prepared from the polymer catalyst and 5 wt% Nafion was immersed in 0.1 M Na<sub>2</sub>SO<sub>4</sub> aqueous solution. The Mott-Schottky analysis was performed on an electrochemical workstation (CHI760E, CH Instrument Corp, Shanghai) using a standard three-electrode cell at room temperature in the dark, with a platinum flag as the counter electrode and a saturated calomel electrode (SCE) as reference. The working electrode prepared from the polymer catalyst and 5 wt% Nafion was immersed in 0.1 M Na<sub>2</sub>SO<sub>4</sub> aqueous solution at pH = ~7 and measured at frequency of 100 Hz.

### 2.4. A general procedure for the photoreductive dehalogenation reactions

The COF-JLU22 (3.0 mg), bromide (0.20 mmol), DIPEA (70 μL, 0.4 mmol) and Hantzsch ester (56 mg, 0.22 mmol) were added into 0.75 mL dry DMF. The mixture was degassed for three times, and then stirred in N<sub>2</sub> under irradiation with a white LED lamp (3.0 W, 1.22 ± 0.01 mW cm<sup>-2</sup>, distance app. 5.0 cm). The reaction was monitored via thin layer chromatography (TLC). After the consumption of the bromide, the COF-JLU22 can be filtered, ethyl acetate was added into the filtrate, and then washed with water for three times, the combined organic layers were dried over MgSO<sub>4</sub>, concentrated in vacuum and purified by column chromatography on a silica gel column using petroleum ether/ethyl acetate (8:1) as an eluent to yield the corresponding products

### 2.5. A general procedure for photocatalytic α-alkylation of aldehydes

To a mixture of COF-JLU22 (3.0 mg), aldehyde (0.75 mmol), bromide (0.25 mmol), 2,6-dimethylpyridine (0.75 mmol) and tetrahydropyrrole (0.05 mmol) were added 2.5 mL anhydrous THF. The mixture was degassed for three times, then stirred under irradiation with light (30 W green LED lamp, distance app. 8.0 cm, 18.4 ± 0.1 mW cm<sup>-2</sup>, or 30 W white LED lamp, distance app. 8.0 cm, 3.0 ± 0.1 mW cm<sup>-2</sup>). The reaction was monitored via TLC. After the

completion of the reaction, the crude mixture was filtrated and dried to determine the NMR yields with 2-phenyl-1,2,3,4-tetrahydroisoquinoline as an internal standard.

### 2.6. Recycle experiment

After the first run reaction was finished, the photocatalyst COF-JLU22 was recovered by centrifugation, and then washed thoroughly with THF and H<sub>2</sub>O to remove any residual products or unreacted substrates. The recovered COF-JLU22 was dried under vacuum at 100 °C overnight. The used photocatalyst COF-JLU22 was re-employed in next cycle under identical conditions.

## 3. Results and discussions

A new imine-linked 2D-COF was constructed under solvothermal conditions via the imine condensation of 1,3,6,8-tetrakis(4-aminophenyl)pyrene (11.3 mg, 0.02 mmol) and 4,4'-(benzothiadiazole-4,7-diyl) dibenzaldehyde (13.7 mg, 0.04 mmol) in a solvent mixture of 1-butanol/o-dichlorobenzene/6 M HOAc (5/5/1, by vol.) at 120 °C for 3 days, which afforded a red solid in 90% isolation yield (Scheme 1). The resulting COF was insoluble in common organic solvents and water. COF-JLU22 was characterized by spectra and analytical methods including Fourier transform infrared (FT-IR), solid state <sup>1</sup>H MAS NMR (Fig. S1) and <sup>13</sup>C CP/MAS NMR, and elemental analysis. Compared with its monomer, the stretching peak of carbonyl group almost completely disappeared in the IR spectrum of the COF. And a stretching peak at 1624 cm<sup>-1</sup> was obtained, indicating the formation of the imine bond (Fig. 1a). More detailed connections of COF-JLU22 were further assessed by <sup>13</sup>C CP/MAS NMR (Fig. 1b). The low-field peaks at about 158 and 150 ppm correspond to the carbon atoms of the –C=N– groups in the formed imine linkage and benzothiadiazole unit, respectively. For other peaks at 138–115 ppm are ascribed to the signals of the substituted and nonsubstituted aromatic carbons. Elemental analysis of the COF-JLU22 showed that the C, H, N, S contents were 78.60, 4.14, 8.85, and 4.93 which were close to the calculated values of 81.19, 3.92, 9.47 and 5.42 expected for an infinite 2D sheet. Thermogravimetric analysis (TGA) demonstrated that the COF-JLU22 has outstanding thermal stability up to 510 °C under nitrogen atmosphere (Fig. S2).

The crystalline structure of COF-JLU22 was investigated by powder X-ray diffraction (PXRD) measurement. As shown in Fig. 2a, the experimental PXRD pattern exhibited a strong diffraction signal at 2.67°, and other relatively weak peaks 3.86°, 5.47°, 8.12°, and 10.98°, which correspond to the (110), (200), (220), (330) and (440) reflections, respectively. The broad signal at higher 2θ (~23.52°) was due to π-π stacking between the layers of COF-JLU22 and assigned to the (001) plane. The structural simulation of the XRD pattern showed that the COF-JLU22 preferably possesses the eclipsed structure (red line). The Pawley refinement showed the XRD profile matched well with the experimentally observed pattern, as proved by their negligible difference

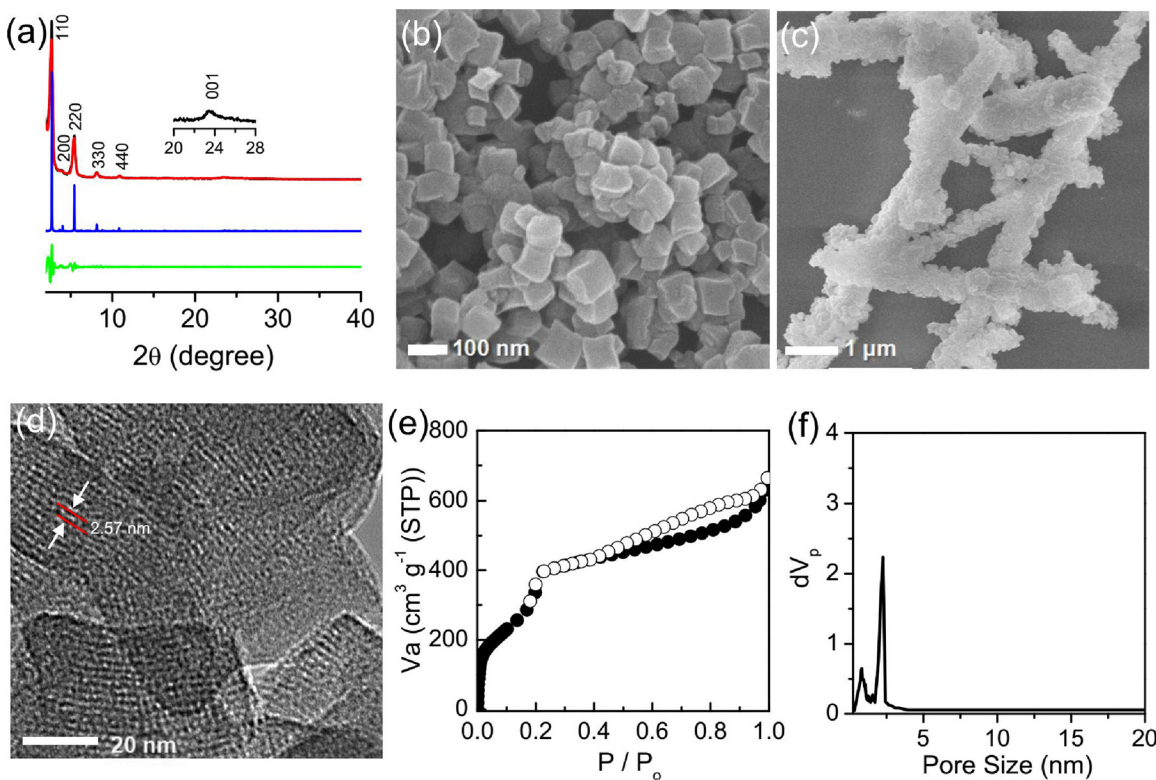


**Fig. 2.** (a) Observed PXRD pattern (black line), the Pawley refined pattern (red line), the difference plot (green line) and the simulated pattern (blue) for the AA stacking model of COF-JLU22. FE-SEM images (b), (c) and HR-TEM image (d) of COF-JLU22. (e) Nitrogen adsorption (point) and desorption (circle) isotherm of COF-JLU22 at 77 K. (f) Pore size distribution of COF-JLU22 on the  $N_2$  adsorption isotherm. (For interpretation of the references to colour in this figure legend, the reader is referred to the web version of this article.)

(green line,  $R_{wp} = 6.74\%$  and  $R_p = 5.56\%$ , respectively). The crystalline morphology of COF-JLU22 was still investigated by field-emission scanning electron microscopy (FE-SEM). The SEM images showed that COF-JLU22 is an irregular block crystal with 60–80 nm size (Fig. 2b), and these nanocrystals are further aggregated into ribbon-shaped structures with lengths in the micrometer size (Fig. 2c). In addition, high-resolution transmission electron microscopy (HR-TEM) images also displayed a polycrystalline structure and long-ordered channels along the *c*-axis (Fig. 2d).

The permanent porosity of COF-JLU22 was investigated by measuring nitrogen gas sorption isotherm of the activated samples at 77 K. As shown in Fig. 2e, the sorption curve was classified as a type IV isotherm according to the IUPAC classification, and exhibited a rapid uptake under at a low relative pressure  $p/p_0 < 0.1$  and a step in range of  $p/p_0 = 0.05–0.20$ , suggesting that COF-JLU22 is a mesoporous material. The Brunauer–Emmett–Teller (BET) surface area of COF-JLU22 was calculated to be  $945 \text{ m}^2 \text{ g}^{-1}$ . The total pore volume was evaluated to be  $1.03 \text{ cm}^3 \text{ g}^{-1}$  at  $p/p_0 = 0.99$ . The pore size distribution from nonlocal density functional theory (NLDFT) showed a dominant pore diameter of 2.36 nm (Fig. 2f), which is close to the theoretical pore size. In addition, we also evaluated the adsorption properties for  $H_2$  of the COF-JLU22 at low pressure and different temperature. And results showed that this COF can uptake  $7.2 \text{ mg g}^{-1}$  of  $H_2$  at 77 K and 1.0 bar, with an isosteric heat ( $Q_{st}$ ) value of  $6.2 \text{ kJ mol}^{-1}$  at low coverage (Fig. S3).

The stability of material is one of the most important parameters for practical applications. Besides thermal stability, therefore, we also tested the chemical and photochemical stability of the new framework. The activated COF-JLU22 samples were immersed in water, different organic solvents including *N,N*-dimethylformamide (DMF), tetrahydrofuran (THF), aqueous HCl (3 M) and NaOH (3 M) solutions at 25 °C for 3 days. To our delight, all collected COF-JLU22 samples

exhibited strong diffraction peaks in XRD patterns without change in the position, and the same skeleton connection in IR profiles (Fig. S4). Even under the additional light irradiation (30 W green LED, 520 nm) for THF suspension of COF-JLU22, the high crystallinity was also retained in the sample after treatment. Thus, these results of the control experiments indicated unambiguously that COF-JLU22 has an excellent thermal and chemical stability as well as photochemical stability.

The electron absorption spectrum of COF-JLU22 in the solid state showed a broad absorption range from the visible light to the near infrared region with a maximum at 510 nm (Fig. 3a). From the Kubelka–Munk-transformed reflectance spectrum, the optical band gap of 2.08 eV could be determined (Fig. 3b). Furthermore, cyclic voltammetry (CV) characterization of COF-JLU22 showed a reversible half wave potential ( $E_{1/2}$ ) at  $-0.86 \text{ V}$  (Fig. S5), which can be assigned to the COF-JLU22<sup>+</sup>/\*COF-JLU22 couple. Corresponding, the potential of valence band (VB) was derived to be  $+1.22 \text{ V}$  (vs. SCE) via extracting the conduction band (CB) value from the optical band gap energy (Fig. 3c). To further determine the relative positions of the CB and VB, the electrochemical Mott–Schottky and VB-XPS experiments were performed. The results of Mott–Schottky measurements indicate that the flat band position ( $V_{fb}$ ) of COF-JLU22 is approximately  $-0.91 \text{ V}$  vs. SCE (Fig. S6). The CB potential is very close to the flat band potential in n-type semiconductors [41,42]. In addition, the VB-XPS spectra (Fig. S7) reveals that the VB edge of COF-JLU22 is located at 1.23 eV [32,43]. Intriguingly, the oxidation/reduction potentials of COF-JLU22 are comparable to those of classical transition metal complexes such as  $[\text{Ru}(\text{bpy})_3]^{3+}$  ( $+1.29 \text{ V}$  vs. SCE) and  $^{*}[\text{Ru}(\text{bpy})_3]^{2+}$  ( $-0.81 \text{ V}$  vs. SCE) [1], implying the promising photoredox capability of the COF-JLU22 for organic transformations.

COF-JLU22 shows large specific surface area, excellent stability, high crystallinity, strong absorption and promising photoredox properties, these features imply that it can serve as an outstanding

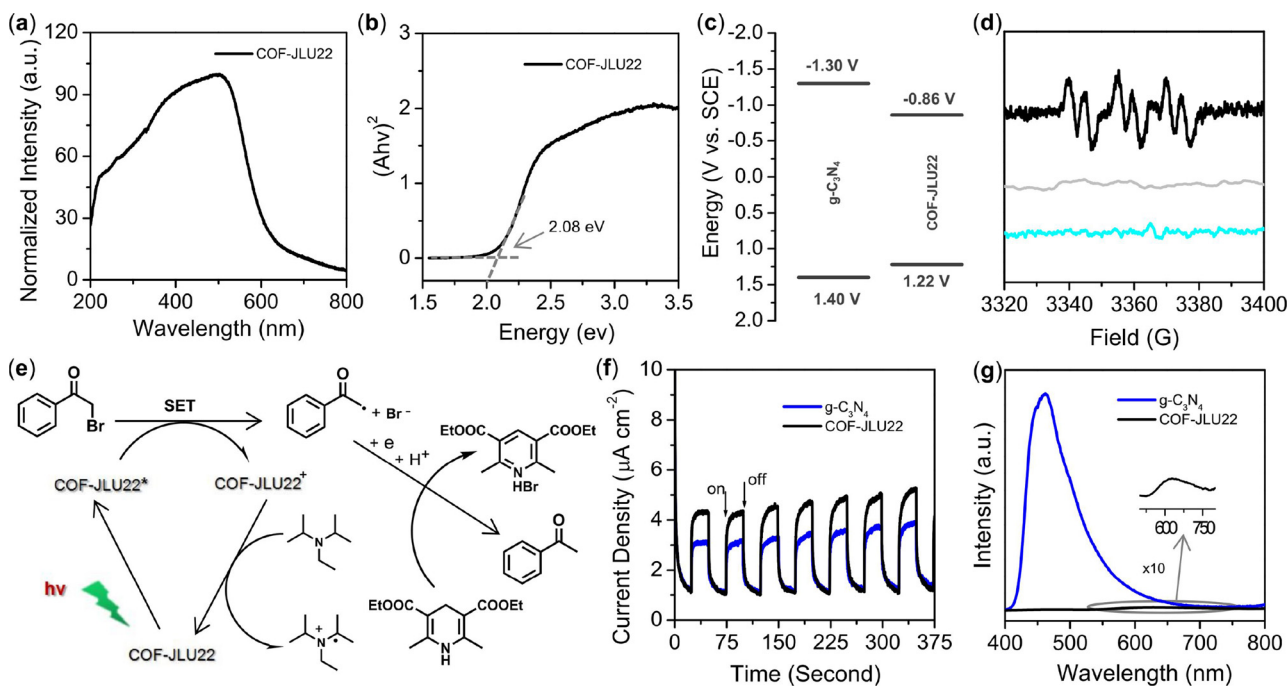


**Fig. 3.** (a) Normalized absorption spectrum of COF-JLU22. (b) Kubelka-Munk-transformed reflectance spectrum of COF-JLU22. (c) Schematic energy band structure of  $g\text{-C}_3\text{N}_4$ <sup>8</sup> and COF-JLU22. (d) EPR spectra of a mixture of COF-JLU22 ( $1.0 \text{ mg mL}^{-1}$ ), diethyl bromomalonate (0.5 M) and PBN solution (0.1 M) in anhydrous DMF in the dark (sky-blue line) and upon light (black line); EPR spectra of a mixture of diethyl bromomalonate (0.5 M) and PBN solution (0.1 M) in anhydrous DMF upon light (gray line). (e) Proposed reaction mechanism for the photoreductive dehalogenation reaction with COF-JLU22. (f) Transient photocurrent responses of  $g\text{-C}_3\text{N}_4$  and COF-JLU22 under visible-light irradiation. (g) The photoluminescence spectra of  $g\text{-C}_3\text{N}_4$  and COF-JLU22 in the solid state. (For interpretation of the references to colour in this figure legend, the reader is referred to the web version of this article.)

**Table 1**  
Photoreductive dehalogenation reaction of phenacyl bromide by COF-JLU22.<sup>a</sup>

Entry	Catalyst	Solvent	Time (h)	Conv. (%) <sup>b</sup>	Yield (%) <sup>b</sup>
1	COF-JLU22	DMF	6	> 99	85
2	COF-JLU22	THF	8	96	78
3	COF-JLU22	CH <sub>3</sub> CN	8	97	74
4 <sup>c</sup>	COF-JLU22	DMF	2	> 99	73
5 <sup>d</sup>	COF-JLU22	DMF	6	3	< 1
6 <sup>e</sup>	COF-JLU22	DMF	6	95	39
7 <sup>f</sup>	COF-JLU22	DMF	6	45	38
8	~	DMF	6	42	15
9	BT-BA	DMF	6	74	42
10	TTA-Py	DMF	6	82	43
11	$g\text{-C}_3\text{N}_4$	DMF	6	74	53
12 <sup>g</sup>	COF-JLU22	DMF	6	91	42

<sup>a</sup> Reaction conditions: COF-JLU22 (3.0 mg),  $\alpha$ -bromoacetophenone (0.20 mmol), Hantzsch ester (0.22 mmol), DIPEA (0.4 mmol), solvent (0.75 mL), N<sub>2</sub>, 3.0 W white LED lamp, 25 °C.

<sup>b</sup> Conversions and yields determined by GC using dodecane as an internal standard.

<sup>c</sup> 30 W green LED lamp 520 nm.

<sup>d</sup> No light irradiation.

<sup>e</sup> No Hantzsch ester.

<sup>f</sup> No DIPEA.

<sup>g</sup> In air.

heterogeneous photocatalyst for organic reactions. We first selected the photoreductive dehalogenation reaction of phenacyl bromide to evaluate the photocatalytic activity of COF-JLU22 under visible-light irradiation. The effect of different solvents on the yield was researched. Irradiation with a white LED lamp (3.0 W), a higher yield (85%) was

obtained in DMF solvent compared with THF and CH<sub>3</sub>CN (Fig. S8 and Table 1, entries 1–3). When using a green LED lamp (520 nm, 30 W) as the light source, the model reaction showed a faster conversion rate, but lower selectivity of the product was achieved (Table 1, entry 4). In addition, the results of control experiments indicated that the light, hydrogen atom source, electron-donating sacrificial agent and photocatalyst COF-JLU22 are all essential for this reaction process (Table 1, entries 5–8). Using two monomers BT-BA and TTA-Py as photocatalysts, the reaction only achieved low yields under optimized conditions (Table 1, entries 9 and 10). The state of art metal-free photocatalyst  $g\text{-C}_3\text{N}_4$  was still studied under the optimized reaction conditions. However, only 53% yield for the target product was obtained (Table 1, entry 11), which indicates the rationality of the structural design for COF-JLU22. When N<sub>2</sub> was replaced with air, phenacyl bromide was hardly converted into the corresponding product (Table 1, entry 12).

In order to confirm the formation of radical species under the photoreductive system, we carried out the research of the formation of radicals by the electron paramagnetic resonance (EPR). The formation of the initial  $\alpha$ -carbonyl radical could be determined in the presence of *N*-tert-butyl- $\alpha$ -phenylnitrone (PBN) as a radical trap under visible light irradiation (Fig. 3d, black line). No signals were observed in the absence of exciting light or COF-based photosensitizer (Fig. 3d, sky-blue and gray lines). On the basis of the above experimental results and previous studies [44], a plausible reaction mechanism for photoreductive dehalogenation reaction over COF-based photocatalyst was proposed. Under visible-light irradiation, the excited state of COF-JLU22 generates photogenerated holes and electrons via charge separation. And the photogenerated hole extracts an electron from the sacrificial agent *N,N*-diisopropylethylamine (DIPEA). Meanwhile, the photogenerated electron transfer from conduction band of COF-JLU22 ( $E_{1/2} = -0.86 \text{ V}$ ) to phenacyl bromide ( $E_{1/2} = -0.49 \text{ V}$ ) [45] resulted in the C–Br cleavage, which gives  $\alpha$ -carbonyl radicals and bromide anions. And then  $\alpha$ -carbonyl radical can abstract a proton and an electron from the Hantzsch ester to form the final product

acetophenone (Fig. 3e).

The separation efficiency and transfer behaviour of photogenerated charge carriers in photocatalyst play important roles in the photocatalytic process. Therefore, we investigated electrochemical tests and photoluminescence spectroscopy to gain insight into them. As shown in Fig. 3f, COF-JLU22 and g-C<sub>3</sub>N<sub>4</sub> exhibited fast photocurrent responses with several repeating cycles of intermittent on-off irradiation, which provided a clear evidence on photoinduced carriers transfer within the polymer frameworks. In comparison with g-C<sub>3</sub>N<sub>4</sub>, COF-JLU22 showed an enhancement of photocurrent density response under visible light irradiation, indicating more effective charge separation in COF-JLU22. Furthermore, photocurrent density did not decay with the increase of illumination time, implying both polymers can provide a stable quantity of photogenerated electrons and holes during light irradiation process. In addition, the photoluminescence spectrum of COF-JLU22 showed an emission peak at 628 nm with very low intensity compared to that of g-C<sub>3</sub>N<sub>4</sub> at 460 nm (Fig. 3g). This reflects that COF-JLU22 possesses the higher separation efficiency of photoinduced electron-hole pairs, which may be attributed to its high crystallinity and  $\pi$ -conjugated skeleton. The efficient generation, migration and separation properties of photogenerated charge pairs for COF-JLU22 and g-C<sub>3</sub>N<sub>4</sub> were in agreement with the experimental results of photocatalysis in dehalogenated reactions (Table 1, entries 1 and 11).

Based on these preliminary results, we further investigated various derivatives of phenacyl bromide bearing electron-donating or electron withdrawing on the phenyl ring as substrates for the photoreductive dehalogenation reaction. Utilizing our optimized reaction conditions, many  $\alpha$ -bromoacetophenones were converted into the corresponding acetophenone compounds with high yields (Table 2, entries 2–8). From

**Table 2**  
Photoreductive dehalogenation reaction of phenacyl bromide and its derivatives by COF-JLU22.<sup>a</sup>

Entry	Substrate	Product	Conv. (%) <sup>b</sup>	Yield (%) <sup>c</sup>
1			> 99	85 <sup>d</sup>
2			> 99	75
3			> 99	77
4			> 99	69
5			> 99	73
6			> 99	75
7			> 99	85
8			> 99	83
9			> 99	88 <sup>d</sup>

<sup>a</sup> Reaction conditions: COF-JLU22 (3.0 mg), substrate (0.20 mmol), DIPEA (0.4 mmol), Hantzsch ester (0.22 mmol), DMF (0.75 mL), N<sub>2</sub>, 3.0 W white LED lamp, 25 °C.

<sup>b</sup> Data were determined by TLC.

<sup>c</sup> Isolated yield by chromatography.

<sup>d</sup> Conversion and yield determined by GC using dodecane as an internal standard.

these catalytic results, we found no inherent relationship between electronic effects of substituents and reaction yields [46]. Furthermore, COF-JLU22 was also capable of photoreducing diethyl-2-bromomalonate to the dehalogenated product in high yield (Table 2, entry 9). Besides the good photocatalytic activity and wide substrate adaptability, the recyclability of the photocatalyst is the most crucial advantage in the solid reaction for commercial applications. Therefore, we investigated the reusability of COF-JLU22 in the photoreductive dehalogenation of phenacyl bromide under visible light irradiation. The COF based heterogeneous photocatalyst was easily separated from the reaction mixtures through centrifugation, washed, dried and reused in the subsequent round of photocatalytic reaction. It was found that COF-JLU22 can be efficiently reused at least five repeating cycles without significant loss of photocatalytic activity (Fig. 4a). To our delight, the COF-JLU22 samples after photocatalysis well retained the original skeleton connectivity (Fig. 4b) and morphology (Fig. 4c). In particular, they still possess high crystallinity and large specific surface area (Fig. 4d and e), which is attributed to the excellent stability of this COF material. In relation to this, we also researched the possibility of a large scale synthesis utilizing phenacyl bromide (0.2 g, 1.0 mmol) as the substrate in 3.75 mL of DMF at 25 °C (Scheme S1). A high yield (80%) was obtained in the scale-up photocatalytic reaction.

Next we also explored that the combination of visible-light solid photoredox catalysis with organocatalysis promotes the formation of carbon–carbon bonds. The enantioselective  $\alpha$ -alkylation of aldehydes developed by MacMillan et al. [47] was selected as a benchmark reaction to demonstrate this proof of concept. Unlike previous reports, we used an achiral amine, tetrahydropyrrole, to replace a chiral secondary amine in our research. Combining a photocatalyst COF-JLU22 and an organocatalyst tetrahydropyrrole, the model reaction of *n*-octylaldehyde and diethyl-2-bromomalonate was carried out with high yield (93%) in THF under irradiation by 30 W green LED lamp (Table S1, entry 1). However, without addition of photocatalyst or organocatalyst, the starting substrates were hardly converted into the corresponding product (Table S1, entries 8 and 11). On the other hand, in the presence of both catalysts and in the absence of light, the reaction scarcely occurred (Table S1, entry 9). In addition, to demonstrate the general applicability of the synergistic photocatalytic system, a series of  $\alpha$ -alkylation reactions between aldehydes and bromides were studied. As shown in Table 3, all reactions displayed high yields. Particularly, when diethyl  $\alpha$ -bromomalonate is used as a reactant, the  $\alpha$ -alkylation reaction has a faster reaction rate and higher yield than those with aromatic bromides. Similar phenomenon was obtained in the reported works and could be attributed to the effect of steric hindrance [48,49]. To further investigate the mechanism of  $\alpha$ -alkylation reactions, some control experiments were conducted. DIPEA as a hole scavenger was added to the reaction mixture under standard conditions, a low yield of 20% for the target product was obtained (Table S1, entry 13). By adding 2,6-di-*tert*-butyl-4-methylphenol as a radical scavenger, similarly, a yield of 25% was achieved (Table S1, entry 14). Based on the results from the control experiments and previous reports, we proposed a plausible mechanism for the  $\alpha$ -alkylation reactions as shown in Fig. S9. Under light irradiation, the polymer COF-JLU22 is excited, and its photogenerated electrons are transferred to the alkyl bromide A, producing the strong oxidizing COF-JLU22<sup>+</sup> and radical B. The radical B adds to the enamine C obtained by condensation of tetrahydropyrrole with aldehyde, and provides the  $\alpha$ -amino radical D. Simultaneously, D is oxidized by the intermediate COF-JLU22<sup>+</sup> yielding the iminium ion E that releases photocatalyst COF-JLU22. Finally, the resulting iminium ion E is converted into target product through hydrolysis process.

Besides the excellent photocatalytic activity and wide substrate adaptability, COF-JLU22 can still exhibit excellent recycling performances in the  $\alpha$ -alkylation reaction. No evidence of important decreasing photocatalytic activity was obtained after reusing COF-JLU22 for five times for the reaction between diethyl-2-bromomalonate and *n*-octylaldehyde (Fig. S10a). In addition, we filtered the COF-based

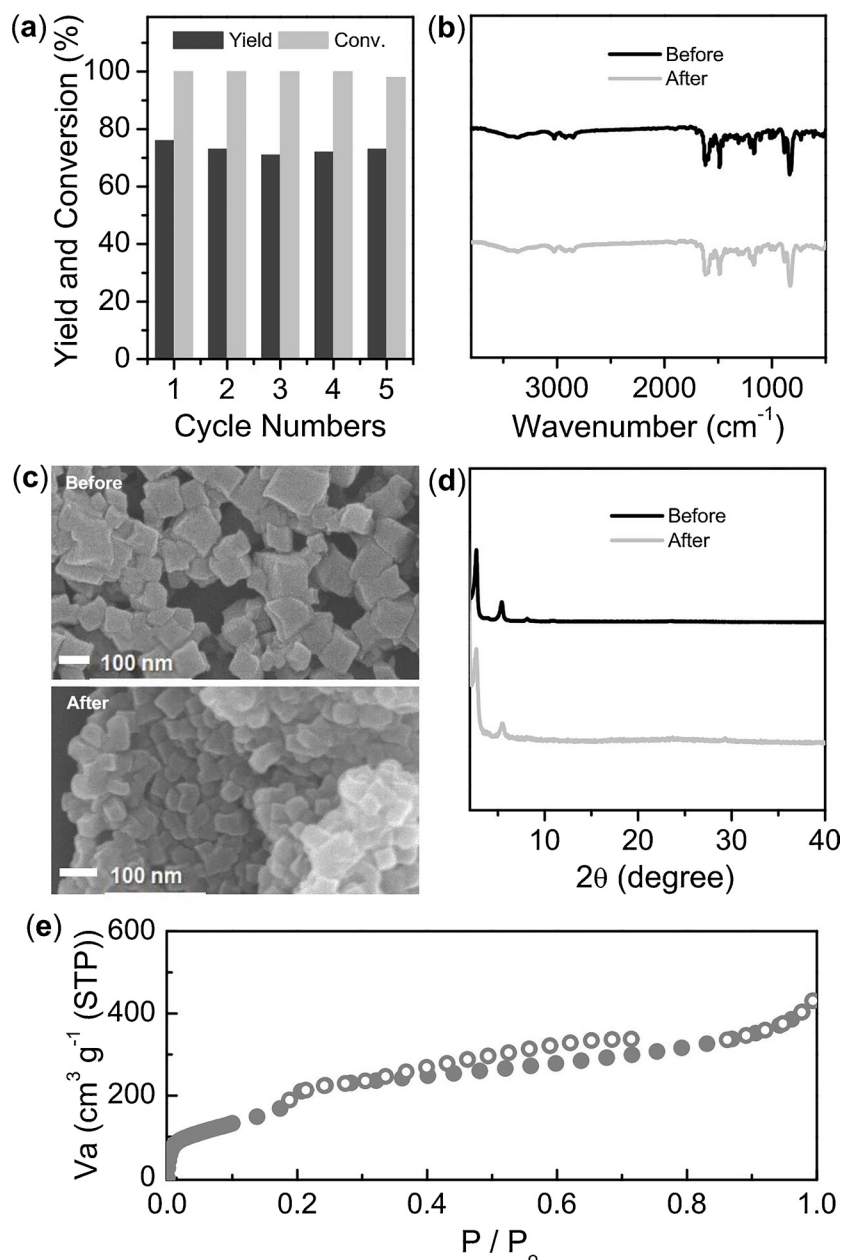


**Fig. 4.** (a) Recycling photoreductive dehalogenation test of phenacyl bromide. (b) FT-IR spectra of COF-JLU22 before and after five runs. (c) SEM images of COF-JLU22 before and after five runs. (d) PXRD curves of COF-JLU22 before and after five runs. (e) Nitrogen adsorption (point) and desorption (circle) isotherm of COF-JLU22 after five runs at 77 K.

photocatalyst from the solution at 69% yield, the isolated solution did not display further photocatalytic reactivity, which clearly indicates the heterogeneous photocatalytic feature of COF-JLU22 (Fig. S10b).

#### 4. Conclusions

In summary, we have developed a photoactive imine-based 2D-COF as a free-metal, heterogeneous photocatalyst for organic synthesis. As well as excellent porosity with a high surface area and pore volume, strong crystallinity, excellent stability, the COF-JLU22 offers an important feature of electron donor and acceptor structure in its extended  $\pi$ -conjugated layers, which results in its wide visible light absorption range and sensitive photoelectric response characteristics. Furthermore, COF-JLU22 can serve as a metal-free, recycle photocatalyst with high catalytic efficiency for reductive dehalogenation of phenacyl bromide derivatives and  $\alpha$ -alkylation of aldehydes under visible-light

irradiation, showing for the first utility of the crystalline 2D-COFs for developing organic photocatalytic reduction systems. Compared with other photoreductive systems based on transition metal and other macromolecule photocatalysts [4,47–49], particularly, this COFs-based system does not contain any toxic metal compounds or residual metal catalysts. We also highlight that this work open up a new way for the design and construction of excellent COFs-based solid photocatalysts at a molecular level. Currently, such explorations are underway in our laboratory.

#### Acknowledgment

This work was supported by the Natural Science Foundation of China (51473064, 21774040 and 61435005).

**Table 3**Photocatalytic  $\alpha$ -alkylation of aldehydes by COF-JLU22.<sup>a</sup>

Entry	aldehyde	bromide	Product	Time (h)	Conv. (%) <sup>b</sup>	Yield (%) <sup>b</sup>
					Tetrahydropyrrrole light, RT	COF-JLU22
1				6	> 99	93
2				6	> 99	90
3				6	> 99	92
4				20 72	99 98 <sup>c</sup>	57 75 <sup>c</sup>
5				20 72	99 92 <sup>c</sup>	62 68 <sup>c</sup>
6				72	> 99 <sup>c</sup>	78 <sup>c</sup>
7				72	> 99 <sup>c</sup>	80 <sup>c</sup>

<sup>a</sup> Reaction conditions: COF-JLU22 (3.0 mg), aldehyde (0.75 mmol), bromide (0.25 mmol), 2,6-dimethylpyridine (0.75 mmol) and tetrahydropyrrrole (0.05 mmol), THF (2.5 mL), N<sub>2</sub>, 30 W green LED lamp (520 nm), 25 °C.

<sup>b</sup> Conversions and yields determined by <sup>1</sup>H NMR using 2-phenyl-1,2,3,4-tetrahydroisoquinoline as an internal standard.

<sup>c</sup> 30 W white LED lamp.

## Appendix A. Supplementary data

Supplementary material related to this article can be found, in the online version, at doi:<https://doi.org/10.1016/j.apcatb.2018.12.065>.

## References

[1] J.M. Narayanan, C.R. Stephenson, Visible light photoredox catalysis: applications in organic synthesis, *Chem. Soc. Rev.* 40 (2011) 102–113.

[2] I. Ghosh, L. Marzo, A. Das, R. Shaikh, B. König, Visible light mediated photoredox catalytic arylation reactions, *Acc. Chem. Res.* 49 (2016) 1566–1577.

[3] L. Shi, W. Xia, Photoredox functionalization of C–H bonds adjacent to a nitrogen atom, *Chem. Soc. Rev.* 41 (2012) 7687–7697.

[4] P. Riente, A.M. Adams, J. Albero, E. Palomares, M.A. Pericàs, Light-driven organocatalysis using inexpensive, nontoxic Bi<sub>2</sub>O<sub>3</sub> as the photocatalyst, *Angew. Chem. Int. Ed.* 53 (2014) 9613–9616.

[5] D.A. Nicewicz, D.W.C. MacMillan, Merging photoredox catalysis with organocatalysis: the direct asymmetric alkylation of aldehydes, *Science* 322 (2008) 77–80.

[6] D.M. Schultz, T.P. Yoon, Solar synthesis: prospects in visible light photocatalysis, *Science* 343 (2014) 1239176.

[7] N.A. Romero, D.A. Nicewicz, Organic photoredox catalysis, *Chem. Rev.* 116 (2016) 10075–10166.

[8] X.C. Wang, S. Blechert, M. Antonietti, Polymeric graphitic carbon nitride for heterogeneous photocatalysis, *ACS Catal.* 2 (2012) 1596–1606.

[9] D. Masih, Y. Ma, S. Rohani, Graphitic C<sub>3</sub>N<sub>4</sub> based noble-metal-free photocatalyst systems: a review, *Appl. Catal. B: Environ.* 206 (2017) 556–588.

[10] T. Zhang, W.B. Lin, Metal-organic frameworks for artificial photosynthesis and photocatalysis, *Chem. Soc. Rev.* 43 (2014) 5982–5993.

[11] Y. Tian, W. Li, C. Zhao, Y. Wang, B. Zhang, Q. Zhang, Fabrication of hollow mesoporous SiO<sub>2</sub>–BiOCl@PANI@Pd photocatalysts to improve the photocatalytic performance under visible light, *Appl. Catal. B: Environ.* 213 (2017) 136–146.

[12] H. Liang, Q. Chen, B. Han, Cationic polycarbazole networks as visible-light heterogeneous photocatalysts for oxidative organic transformations, *ACS Catal.* 8 (2018) 5313–5322.

[13] R. Li, J. Byun, W. Huang, C. Ayed, L. Wang, K.A.I. Zhang, Poly(benzothiadiazoles) and their derivatives as heterogeneous photocatalysts for visible-light-driven chemical transformations, *ACS Catal.* 8 (2018) 4735–4750.

[14] W.L. He, C.D. Wu, Incorporation of Fe-phthalocyanines into a porous organic framework for highly efficient photocatalytic oxidation of arylalkanes, *Appl. Catal. B: Environ.* 234 (2018) 290–295.

[15] Y. Zhi, K. Li, H. Xia, M. Xue, Y. Mu, X. Liu, Robust porous organic polymers as efficient heterogeneous organo-photocatalysts for aerobic oxidation reactions, *J. Mater. Chem. A: Mater. Energy Sustain.* 5 (2017) 8697–8704.

[16] W. Zhang, J. Tang, W. Yu, Q. Huang, Y. Fu, G. Kuang, C. Pan, G. Yu, Visible light-driven C–3 functionalization of indoles over conjugated microporous polymers, *ACS Catal.* 8 (2018) 8084–8091.

[17] Y. Zhi, S. Ma, H. Xia, Y. Zhang, Z. Shi, Y. Mu, X. Liu, Construction of donor-acceptor type conjugated microporous polymers: a fascinating strategy for the development of efficient heterogeneous photocatalysts in organic synthesis, *Appl. Catal. B: Environ.* 244 (2019) 36–44.

[18] X. Feng, X. Ding, D. Jiang, Covalent organic frameworks, *Chem. Soc. Rev.* 41 (2012) 6010–6022.

[19] Z. Li, X. Feng, Y. Zou, Y. Zhang, H. Xia, X. Liu, Y. Mu, A 2D azine-linked covalent organic frameworks for gas storage applications, *Chem. Commun.* 50 (2014) 13825–13828.

[20] Y. Zeng, R. Zou, Y. Zhao, Covalent organic frameworks for CO<sub>2</sub> capture, *Adv. Mater.* 28 (2016) 2855–2873.

[21] S. Dalapati, S. Jin, J. Gao, Y. Xu, A. Nagai, D. Jiang, An azine-linked covalent organic framework, *J. Am. Chem. Soc.* 135 (2013) 17310–17313.

[22] Z. Li, Y. Zhang, H. Xia, Y. Mu, X. Liu, A robust and luminescent covalent organic framework as a highly sensitive and selective sensor for the detection for Cu<sup>2+</sup> ions, *Chem. Commun.* 52 (2016) 6613–6616.

[23] Y. Zhang, X. Shen, X. Feng, H. Xia, Y. Mu, X. Liu, Covalent organic frameworks as pH responsive signaling scaffolds, *Chem. Commun.* 52 (2016) 11088–11091.

[24] S. Wang, Q. Wang, P. Shao, Y. Han, X. Gao, L. Ma, S. Yuan, X. Ma, J. Zhou, X. Feng, B. Wang, Exfoliation of covalent organic frameworks into few-layer redox-active nanosheets as cathode materials for lithium-ion batteries, *J. Am. Chem. Soc.* 139 (2017) 4258–4261.

[25] H. Xu, J. Gao, D. Jiang, Stable, crystalline, porous, covalent organic frameworks as a platform for chiral organocatalysts, *Nat. Chem.* 7 (2015) 905–912.

[26] X. Wang, X. Han, J. Zhang, X. Wu, Y. Liu, Y. Cui, Homochiral 2D porous covalent organic frameworks for heterogeneous asymmetric catalysis, *J. Am. Chem. Soc.* 138

(2016) 12332–12335.

[27] S. Lin, C.S. Diercks, Y.B. Zhang, N. Kornienko, E.M. Nichols, Y. Zhao, A.R. Paris, D. Kim, P. Yang, O.M. Yaghi, C.J. Chang, Covalent organic frameworks comprising cobalt porphyrins for catalytic  $\text{CO}_2$  reduction in water, *Science* 349 (2015) 1208–1213.

[28] S. Ding, J. Gao, Q. Wang, Y. Zhang, W. Song, C. Su, W. Wang, Construction of covalent organic framework for catalysis: Pd/COF-LZU1 in Suzuki–Miyaura coupling reaction, *J. Am. Chem. Soc.* 133 (2011) 19816–19822.

[29] Y. Zhi, P. Shao, X. Feng, H. Xia, Y. Zhang, Z. Shi, Y. Mu, X. Liu, Covalent organic frameworks: efficient, metal-free, heterogeneous organocatalysts for chemical fixation of  $\text{CO}_2$  under mild conditions, *J. Mater. Chem. A: Mater. Energy Sustain.* 6 (2018) 374–382.

[30] J. Guo, Y. Xu, S. Jin, L. Chen, T. Kaji, Y. Honsho, M.A. Addicoat, J. Kim, A. Saeki, H. Ihee, S. Seki, S. Irle, M. Hiramoto, J. Gao, D. Jiang, Conjugated organic framework with three-dimensionally ordered stable structure and delocalized  $\pi$  clouds, *Nat. Commun.* 4 (2013) 2736.

[31] Y. Fu, X. Zhu, L. Huang, X. Zhang, F. Zhang, W. Zhu, Azine-based covalent organic frameworks as metal-free visible light photocatalysts for  $\text{CO}_2$  reduction with  $\text{H}_2\text{O}$ , *Appl. Catal. B: Environ.* 239 (2018) 46–51.

[32] S. He, B. Yin, H. Niu, Y. Cai, Targeted synthesis of visible-light-driven covalent organic framework photocatalyst via molecular design and precise construction, *Appl. Catal. B: Environ.* 239 (2018) 147–153.

[33] M. Liu, Q. Huang, S. Wang, Z. Li, B. Li, S. Jin, B. Tan, Crystalline covalent triazine frameworks by *in situ* oxidation of alcohols to aldehyde monomers, *Angew. Chem. Int. Ed.* 57 (2018) 11968–11972.

[34] P. Pachfule, A. Acharjya, J. Roeser, T. Langenhahn, M. Schwarze, R. Schomäcker, A. Thomas, J. Schmidt, Diacetylene functionalized covalent organic framework (COF) for photocatalytic hydrogen generation, *J. Am. Chem. Soc.* 140 (2018) 1423–1427.

[35] L. Stegbauer, K. Schwinghammer, B.V. Lotsch, A hydrazone-based covalent organic framework for photocatalytic hydrogen production, *Chem. Sci.* 5 (2014) 2789–2793.

[36] Y. Zhi, Z. Li, X. Feng, H. Xia, Y. Zhang, Z. Shi, Y. Mu, X. Liu, Covalent organic frameworks as metal-free heterogeneous photocatalysts for organic transformations, *J. Mater. Chem. A: Mater. Energy Sustain.* 5 (2017) 22933–22938.

[37] P. Wei, M. Qi, Z. Wang, S. Ding, W. Yu, Q. Liu, L. Wang, H. Wang, W. An, W. Wang, Benzoxazole-linked ultrastable covalent organic frameworks for photocatalysis, *J. Am. Chem. Soc.* 140 (2018) 4623–4631.

[38] Y. Wu, H. Xu, X. Chen, J. Gao, D. Jiang, A  $\pi$ -electronic covalent organic framework catalyst:  $\pi$ -walls as catalytic beds for Diels–Alder reactions under ambient conditions, *Chem. Commun.* 51 (2015) 10096–10098.

[39] F. Auras, L. Ascherl, A.H. Hakimioun, J.T. Margraf, F.C. Hanusch, S. Reuter, D. Bessinger, M. Döblinger, C. Hettstedt, K. Karaghiosoff, S. Herbert, P. Knochel, T. Clark, T. Bein, Synchronized offset stacking: a concept for growing large-domain and highly crystalline 2D covalent organic frameworks, *J. Am. Chem. Soc.* 138 (2016) 16703–16710.

[40] D. Bessinger, L. Ascherl, F. Auras, T. Bein, Spectrally switchable photodetection with near-infrared-absorbing covalent organic frameworks, *J. Am. Chem. Soc.* 139 (2017) 12035–12042.

[41] W. Jiang, Q. Ruan, J. Xie, X. Chen, Y. Zhu, J. Tang, Oxygen-doped carbon nitride aerogel: a self-supported photocatalyst for solar-to-chemical energy conversion, *Appl. Catal. B: Environ.* 236 (2018) 428–435.

[42] G. Liu, G. Zhao, W. Zhou, Y. Liu, H. Pang, H. Zhang, D. Hao, X. Meng, P. Li, T. Kako, J. Ye, In situ bond modulation of graphitic carbon nitride to construct p–n homojunctions for enhanced photocatalytic hydrogen production, *Adv. Funct. Mater.* 26 (2016) 6822–6829.

[43] H. Yu, R. Shi, Y. Zhao, T. Bian, Y. Zhao, C. Zhou, G.I.N. Waterhouse, L.Z. Wu, C.H. Tung, T. Zhang, Alkali-assisted synthesis of nitrogen deficient graphitic carbon nitride with tunable band structures for efficient visible-light-driven hydrogen evolution, *Adv. Mater.* 29 (2017) 1605148.

[44] Z.J. Wang, S. Ghasimi, K. Landfester, K.A.I. Zhang, A conjugated porous polybenzobisthiadiazole network for a visible light-driven photoredox reaction, *J. Mater. Chem. A: Mater. Energy Sustain.* 2 (2014) 18720–18724.

[45] D.D. Tanner, H.K. Singh, Reduction of  $\alpha$ -halo ketones by organotin hydrides. An electron-transfer-hydrogen atom abstraction mechanism, *J. Org. Chem.* 51 (1986) 5182–5186.

[46] J. Lee, J.W. Papatzimas, A.D. Bromby, E. Gorobets, D.J. Derkens, Thiaphorphyrin-mediated photocatalysis using red light, *RSC Adv.* 6 (2016) 59269–59272.

[47] H. Shih, M.N.V. Wal, R.L. Grange, D.W.C. MacMillan, Enantioselective  $\alpha$ -benzylation of aldehydes via photoredox organocatalysis, *J. Am. Chem. Soc.* 132 (2010) 13600–13603.

[48] W. Huang, B.C. Ma, D. Wang, Z.J. Wang, R. Li, L. Wang, K. Landfester, K.A.I. Zhang, A fixed-bed photoreactor using conjugated nanoporous polymer-coated glass fibers for visible light-promoted continuous photoredox reactions, *J. Mater. Chem. A: Mater. Energy Sustain.* 5 (2017) 3792–3797.

[49] J. Luo, X. Zhang, J. Zhang, Carbazolic porous organic framework as an efficient, metal-free visible-light photocatalyst for organic synthesis, *ACS Catal.* 5 (2015) 2250–2254.